

LLNL X-BAND RF GUN RESULTS*

R. A. Marsh[†], G. G. Anderson, D. J. Gibson, C. P. J. Barty,
 Lawrence Livermore National Laboratory, Livermore, CA USA 94550
 Y. Hwang, University of California, Irvine, CA USA 92697

Abstract

An X-band test station and Inverse Compton Scattering (ICS) x-ray source has been built and commissioned at Lawrence Livermore National Laboratory (LLNL). The electron beam source is a unique 5.59 cell RF photoinjector, which will be described in detail, including: quantum efficiency, emittance measurements, energy spread and jitter, final focus spot size and stability, laser profile and final transport, and consistency with expectations based on beam dynamics simulations.

INTRODUCTION

Accelerator-based x-ray and gamma-ray sources are expanding rapidly, with several large facilities in construction both in Japan and in Europe [1,2]. LLNL has a successful history utilizing gamma-rays generated by a linac-driven, laser-based Compton scattering gamma-ray source [3–6]. Next generation advancements in linac-based x-ray and gamma-ray production require increasing the average flux of gamma-rays at a specific energy (that is, $N/eV/sec$ at the energy of interest). One way to accomplish this is to increase the effective repetition rate by operating the RF photoinjector in a multi-bunch mode, accelerating multiple electron bunches per RF macro-pulse. This multi-bunch mode will have stringent requirements for the electron bunch properties including low emittance and energy spread, but across multiple bunches. An X-band test station has been built and commissioned at LLNL to develop multi-bunch electron beams and generate x-rays. This paper summarizes electron beam results from the initial optimization of the X-band RF photoinjector performance.

Building on the design work for a 250 MeV gamma-ray source, and leveraging hardware and engineering done for the VELOCIRAPTOR X-band accelerator [7], LLNL established an X-band test station for laser-Compton research and development. The current test station parameters are summarized in Table 1. Beam dynamics are summarized in Fig. 1 for a 100 pC bunch generated in the Mark 1 X-band RF gun and accelerated by a single T53 traveling wave accelerating section. The current goals of the test station efforts are first x-ray demonstration, initial x-ray application experiments, electron beam optimization, demonstration of multiple electron bunches spaced as close as every RF bucket, and upgraded controls systems. Success has been achieved on all of these fronts, with preliminary results reported in [8,9] and elsewhere at this conference [10,11].

* This work performed under the auspices of the U.S. Department of Energy by Lawrence Livermore National Laboratory under Contract DE-AC52-07NA27344.

[†] marsh19@llnl.gov

Table 1: LLNL Test Station Parameters

Charge	10–400 pC
Bunch duration	2 ps
Bunch rise/fall	<250 fs
Normalized emittance	$\lesssim 0.5$ mm mrad
Gun energy	7 MeV
Cathode field	185 MV/m
Section gradient	~ 50 MV/m
Final energy	30 MeV

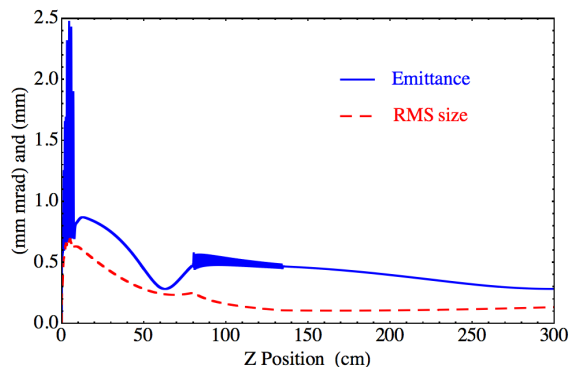


Figure 1: PARMELA beam dynamics simulation for a bunch charge of 100 pC.

TEST STATION

The accelerator is built around a state-of-the-art X-band RF photoinjector [12]. RF power is provided by a 50 MW 11.424 GHz SLAC built XL4 klystron powered by a solid-state Scandinova modulator [13]. The high voltage modulator and X-band tube reside in a separate area with RF distribution fed through a hole in the wall to the linear accelerator. A manifold divides the power between the RF gun and the accelerating sections [14]. The RF power provided is of very high phase and power stability, providing excellent electron beam consistency. A 5.59 cell RF gun incorporates LCLS S-band gun improvements, producing 7 MeV sub-micron emittance bunches in excess of 100 pC. A SLAC designed T53 traveling wave accelerating section is used to boost the energy from 7 MeV to a maximum of up to 31 MeV. The T53VG3MC is a traveling wave section with a group velocity of 3 percent of the speed of light, with mode converter couplers [15]. The mode converter couplers on these section have been redesigned to incorporate an RF dipole and quadrupole canceling racetrack shape. A second T53 accelerating section has been installed to further increase the energy reach of the test station, and will be commissioned at the end of the year. Beam steering uses X-Y windowpane



Figure 2: Photograph of X-band test accelerator in the south cave of B194 at LLNL.

dipole magnets. Two quadrupole triplets focus the beam for transport, final focus for the laser interaction, and are used for quad-scan emittance measurement. A chicane is used to shield x-ray experiments from dark current and allow for an interaction laser exit path. The electron beam energy is measured with a dipole magnet that has been calibrated to serve as a spectrometer, and captured in a shielded dump. Other diagnostics include ICTs, YAG screens, and OTR measurements. The X-band accelerator is shown in Figure 2.

Laser

The Photocathode Drive Laser, which generates the electron beam is a chirped pulse amplification system, based on Ti:Sapphire that is shared with the main S-band 100 MeV accelerator facility. This laser provides up to 20 mJ of uncompressed 780 nm laser light which is transported to the accelerator, where a dedicated compressor and frequency tripler compresses the pulse to 200 fs. Typically, 3 μJ of UV light is used to illuminate the cathode, but up to 150 μJ is currently available. The beam is then apertured to provide a sharp radial edge, typically with a 0.5 mm diameter. The apertured beam is then relay imaged to the photoinjector cathode. In order to generate multiple pulses, a hyper-Michelson pulse stacker [16] is used.

RESULTS

The commissioning of the test station took place in stages: initial testing of the high voltage modulator and klystron, RF conditioning of the T53 section to 25 MW and 200 ns, RF conditioning of the Mark 1 RF gun to 200 MV/m gradient, electron beam production and tuning, and finally x-ray production and characterization. Arc detection is active on the klystron forward and reverse power, as well as the RF gun and accelerator section reverse power traces, with current advances in the control systems reported in [10]. First beam was observed on the initial phase scan with photocathode laser illumination, attributed to precision alignment of the beamline components.

Schotky scans of the charge measured on the calibrated ICT with respect to RF phase are used to set the laser to RF phase and measure quantum efficiency (QE). The RF gun is currently tuned for an RF phase of 30° from zero crossing, and has been stable in day-to-day operations to within a few degrees. A relatively long LMR cable phase locks the X-band RF signal with respect to the photocathode drive laser, but temperature stability of this line has not had a significant impact. A photocathode laser energy of 3 μJ is often used and yields ~ 40 pC of charge for a QE of $\sim 5 \times 10^{-5}$, and has been observed to be relatively stable. Pointing and centering loops have been implemented in the ultraviolet to maintain the transport alignment from the stretcher to the compressor and tripler and these have resulted in improved stability of the delivered laser energy. The laser transverse profile is maintained by centering the UV pulse on an aperture, and this is tuned throughout the day to maintain the transverse profile and energy.

The electron beam emittance is measured using the standard quadrupole scan technique [17] with the quadrupole triplet upstream of the final focus and a YAG screen with a reasonable drift length. The electron beam has been tuned for minimal emittance by varying the gun emittance compensation solenoid field, cathode gradient, laser position on the cathode, laser transverse profile, laser timing, RF phase, accelerator section phase, steering, and ultimately even the transverse position of the gun when consistent data showed a $\sim 200 \mu\text{m}$ misalignment of the RF gun with respect to the solenoid. Rapid emittance measurements were made possible by significant architecture improvements to the controls system and diagnostics, which also enabled rapid retuning of the machine [10]. An emittance of $0.3 \mu\text{m}$ has been measured at a charge of 88 pC, in agreement with *PARMELA* predictions for 100 pC bunch charge. Emittances as low as $0.1 \mu\text{m}$ have been measured at low charge, and charges of up to 400 pC have also been measured at higher emittance.

The electron beam energy is measured by a spectrometer at the end of the beamline. A large bending dipole has been calibrated using a gauss probe scan along the beam path and correlating the field integral to both a gauss probe mounted external to the dipole vacuum chamber and beam dynamics

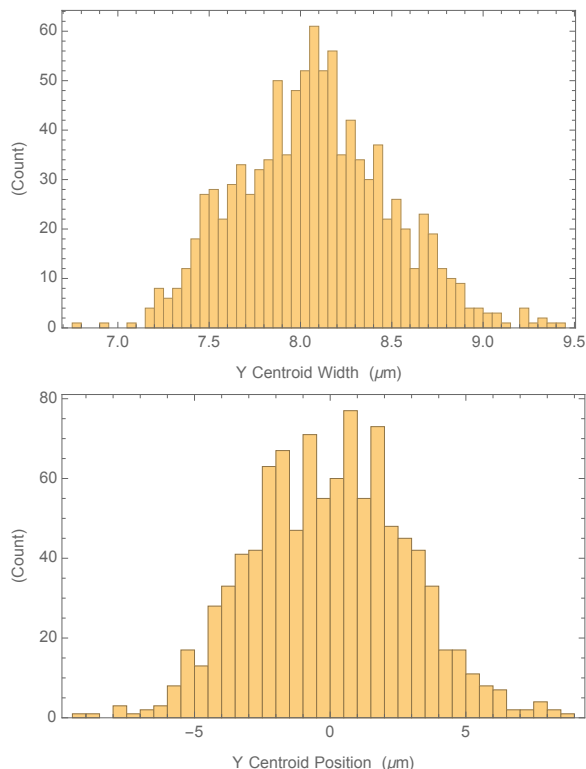


Figure 3: Histograms of final focus measured with OTR: RMS width of 8 μm and jitter of 3 μm .

simulations to determine the electron beam energy [18]. The beam is viewed on a YAG screen, which has been calibrated using the beam at varying dipole currents and observing the range of movement. Energy spread has been consistent on the order of 0.03%, and an observed energy jitter of order 0.07% is currently being investigated so that it can be understood and eliminated. The vertical position jitter is also used to measure the scale of final focus pointing jitter by scaling the quadrupole triplet current down and observing the negligible increase in vertical centroid spread.

The final focus is measured by optical transition radiation (OTR) in the interaction region chamber. A spot size of 8 μm vertical and 10 μm horizontal has been measured with jitter on the order of 3 μm and 5 μm respectively, with histograms for the vertical direction shown in Figure 3. For Laser-Compton x-ray production the long pulse interaction laser overlaps well in the current design of the interaction region, and the measured jitter doesn't significantly decrease the photon flux. Electron beam measurements including jitter are used to model the predicted x-ray flux accurately.

Electron beam optimization has been a major component of the current effort, both to achieve the lowest emittance possible and to generate the brightest x-rays for imaging

experiments. First electron beam was followed by first x-ray beam a year later. New interaction laser optics and realignment of the x-ray camera have produced excellent x-ray results, with precision calibration to determine how close the photon flux matches predictions as presented in [11].

CONCLUSION

The LLNL laser-Compton source is operational and now offers a valuable test bed to optimize all areas of source development. Great initial success in producing laser-Compton x-rays, and using multiple bunches to increase x-ray flux are an important first step in increasing photon flux. The controls system for the test station is continuing to be upgraded to make operation of the accelerator easier and more robust. X-ray production and k-edge imaging in close agreement with theory are exciting results at 30 keV energies. Commissioning of the second T53 accelerator section will enable higher energy x-rays in the next year.

REFERENCES

- [1] *Nuclear Physics and Gamma-ray Sources for Nuclear Security and Nonproliferation*, World Scientific Publishing Co. Ltd., Singapore (2015).
- [2] *Technical Design Report EuroGammaS proposal for the ELI-NP Gamma beam System*, <http://arxiv.org/abs/1407.3669> (2014).
- [3] C.P.J. Barty, and F.V. Hartemann, **UCRL-TR-206825** (2004).
- [4] F. Albert, *et al.*, *Opt. Lett.* **35**, 354 (2010).
- [5] D.J. Gibson, *et al.*, *Phys. Rev. STAB* **13**, 070703 (2010).
- [6] F. Albert, *et al.*, *Phys. Rev. STAB* **13**, 070704 (2010).
- [7] S.G. Anderson, *et al.*, *Nucl. Instrum. Methods Phys. Res., Sect. A*, **657** 1, pp. 140–149 (2011).
- [8] D.G. Gibson, *et al.*, *IPAC 2015*, **TUBC2**.
- [9] R. A. Marsh, *et al.*, *IPAC 2015*, **TUPMA025**.
- [10] D. J. Gibson, *et al.*, *IPAC 2016*, **THPOW027**.
- [11] Y. Hwang, *et al.*, *IPAC 2016*, **TUPOW052**.
- [12] R.A. Marsh, *et al.*, *Phys. Rev. ST Accel. Beams*, **15**, 102001 (2012).
- [13] R.A. Marsh, *et al.*, *IPAC 2013*, **WEPFI078**.
- [14] R.A. Marsh, *et al.*, *PAC 2011*, **TUP132**.
- [15] C. Adolphsen, *PAC 2003*, **ROPC006**.
- [16] C.W. Siders, *et al.*, *Appl. Opt.* **37**, 5302 (1998).
- [17] C. Limborg, S. Gierman, and J. Power, *PAC 2003*, **WGG03**.
- [18] P. Yeh, University of California, Irvine, Masters thesis (2015).